Available online at www.sciencedirect.com
SCIENCE DIRECT®
Coordination Chemistry Reviews 248 (2004) 1271–1276
COORDINATION CHEMISTRY REVIEWS
www.elsevier.com/locate/ccr

Review

Core–shell nanoporous electrode for dye sensitized solar cells: the effect of shell characteristics on the electronic properties of the electrode

Yishay Diamant, Shlomit Chappel, S.G. Chen, Ophira Melamed, Arie Zaban*

Department of Chemistry, Bar-Ilan University, Ramat-Gan 52900, Israel

Received 19 November 2003; accepted 17 March 2004
Available online 7 May 2004

Contents

Abstract

Nanoporous TiO_2 electrodes coated with a thin layer of various wide band gap materials were tested in dye sensitized solar cells (DSSCs). Using Nb_2O_5, ZnO, $SrTiO_3$, ZrO_2, Al_2O_3 and SnO_2 as shell materials, we find that the mechanism by which the shell affects the electrode properties depends on the coating material. In the exceptional case of Nb_2O_5, the coating forms a surface energy barrier, which slows the recombination reactions. The other shell materials each form a surface dipole layer that shifts the conduction band potential of the core TiO_2. The shift direction and magnitude depend on the dipole parameters which are induced by the properties of the two materials at the core–shell interface. The results show that either the shell acidity or the electron affinity of the shell are the shift controlling parameters, although the former seems more likely. This new tool for the modification of the electronic properties of the nanoporous electrodes allows for optimization towards a wide range of applications.

Keywords: Core–shell nanomaterials; Nanoporous electrode; Sensitized solar cells

1. Introduction

Dye sensitized solar cells (DSSCs) are based on the photo-injection of electrons from dye molecules into an inorganic semiconductor and holes transport by a redox mediator [1]. The nanoporous structure of the inorganic semiconductor provides the large surface area necessary to achieve significant optical density of the solar cell despite the low light absorption of a dye monolayer [1–4]. However, the porous electrode also plays an important role in the enhancement of recombination processes in the DSSC, thus decreasing all cell parameters and its total conversion efficiency [5–7]. Since the electrolyte penetrates throughout the entire porous structure, a large surface area is available for a reaction between the photoinjected electrons in the semiconductor

* Corresponding author. Tel.: +972-35317876; fax: +972-35351250.
E-mail address: zabana@mail.biu.ac.il (A. Zaban).

0010-8545/$ – see front matter © 2004 Elsevier B.V. All rights reserved.
doi:10.1016/j.ccr.2004.03.003

and the oxidized ions in the redox mediator or oxidized dye at the semiconductor surface [5,8]. Under operating conditions, the electrons are required to diffuse several micrometers in the semiconductor surrounded by electron acceptors at a distance of only several nanometers. The small size of the semiconductor crystals allows only limited band bending at electrode surface, thus in this system there is no electric field that can assist the separation of the electrons in the semiconductor from their image charge acting as an energy barrier of the recombination processes [5,7,9,10].

The literature reveals an increasing interest in a new design of the nanoporous electrode which is based on the core–shell configuration [11–22]. These electrodes can slow the recombination processes by the formation of an energy barrier at the TiO_2 surface. The core–shell nanoporous electrode consists of a nanoporous inorganic semiconductor matrix that is covered with a shell of other metal oxide. The conduction band potential of the shell should be more negative than that of the core semiconductor in order to generate an energy barrier for the reaction of the electrons present in the core with the oxidized dye or the redox mediator in solution. Two fabrication approaches of the nanoporous core–shell electrodes are reported in the literature. The first approach involves synthesis of core–shell nanoparticles that are applied onto the conducting substrate [11–16]. The consequence of this fabrication method is the formation of an energy barrier not only at the electrode/electrolyte interface but also between the individual particles of the core semiconductor. Thus, at least conceptually, the resistance to the transport of the photoinjected electrons through the core network should increase. In the second approach, a nanoporous core electrode that is made first, serves as a matrix for coating of the thin shell layer [17–22]. Here, the core particles are connected directly to each other allowing electron transport through single material.

In our previous reports we developed the second fabrication method for several core and shell materials [19–22]. In some core–shell combinations, e.g. TiO_2 core–Nb_2O_5 shell or SnO_2 core–TiO_2 shell, indeed the coating formed an energy barrier at the electrode surface. This energy barrier led to improvement of all solar cell parameters resulting in 35% increase of the overall conversion efficiency [19–21]. In other core–shell combinations we found that the coating affects the electrode properties by a different mechanism. The shell material shifts the conduction band potential of the core rather than forming an energy barrier. For example, coating of TiO_2 with a $SrTiO_3$ shell resulted in a shift of the TiO_2 conduction band in the negative direction. Consequently, introduction of a $SrTiO_3$ coated TiO_2 electrode to DSSC increased the open circuit photovoltage while reducing the short circuit photocurrent compare to the non-coated TiO_2 electrode [22].

In this work, we extended our investigations to a large range of shell materials: $SrTiO_3$, ZnO, SnO_2, ZrO_2 and Al_2O_3. These shell materials cover a conduction band potential range starting positive of the TiO_2 core, through values that are significantly more negative than that of the TiO_2. Moreover this potential range covers the excited state potential of the dye, which is lower than the conduction band potentials of both ZrO_2 and Al_2O_3. Consequently, this material choice should provide the basic understanding of the core–shell nanoporous electrode.

The purpose of this study is to address two issues: One, directly related to the DSSCs, examines the effect of the shell material on the performance of the solar cell. Two, to study the ability to modify the electronic properties of metal oxide nanocrystals by inorganic materials. Here we utilize the porous electrode geometry that permits solvent penetration throughout its volume, in order to electrically approach the single nanoparticle while in solution.

The core–shell systems were examined using photovoltage spectroscopy, spectro-electrochemistry and DSSCs measurements under illumination and in the dark. The DSSC measurements refer to current–voltage dependence (*I–V*) and incident photon to current efficiency (IPCE). The results show that all coatings examined in this study affect the core material by the conduction band shift mechanism rather than the formation of an energy barrier at the surface. The shift is explained by the formation of a dipole layer at the core–shell interface. The magnitude and direction of the conduction band potential shift is therefore dependent on the magnitude and direction of the surface dipole formed by the coating.

2. Experimental

2.1. Electrode preparation

The nanoporous TiO_2 electrode was fabricated on conductive glass substrates (Libby Owens Ford, 8 Ω/□ F-doped SnO_2) using anatase crystals of average 23 nm diameter, as described elsewhere [22]. Film thickness of 4 μm was measured with Surftest SV 500 profilometer (Mitutoyo Co). The ZnO coat of the TiO_2 film was done by electrochemical deposition in a three-electrode cell. The deposition solution consisted of 0.15 M $LiNO_3$, 0.005 M $Zn(NO_3)_2$ hydrate and 0.05 M $ZnCl_2$ in propylene carbonate based on a procedure reported in the literature [23] The potential applied to the TiO_2 working electrode was scanned at 50 mV/s for one cycle between 0 and −1.4 V versus an Ag/AgCl reference electrode. This procedure yielded the largest effect on the DSSC performance.

The other shell coatings were preformed by dipping of the TiO_2 electrode in solution containing a precursor of each oxide. For each core–shell system the largest effect on the DSSCs performance was observed for the following coating procedures. $SrTiO_3$, 45 s dipping in 5 mM strontium oxide in dry ethanol [22]. Al_2O_3, 600 s in 5 mM aluminum chloride in ethanol and ether solution (1:1 volume ratio). Nb_2O_5, 30 s in 5 mM Nb(isopropoxide)$_5$ in dry isopropanol [20]. ZrO_2, 8 h in 5 mM Zr(isopropoxide)$_4$ in dry isopropanol. SnO_2, 30 s in 50 mM Sn(isopropoxide)$_4$ in dry isopropanol [21].

After coating, the electrodes were sintered at the temperature that was found to yield the best performance in the DSSCs. The ZnO and the SnO_2 coated TiO_2 electrodes were sintered for 30 min at 380 and 500 °C, respectively. The other core–shell electrodes were sintered at 550 °C for 30 min.

The dye adsorption was carried out by over night dipping in dry ethanol containing 0.5 mM of the N3 dye (*cis*-di(isothiocyanato)-*N*-bis(4,4′-dicarboxy-2,2′-bipyridine) ruthenium(II)) (Solaronix SA). The electrode was dried at 150 °C and soaked at 80 °C to maintain the dry conditions.

2.2. Measurements

Spectro-electrochemical measurements were performed in a three-electrode Teflon cell using HP 8453 spectrophotometer. The porous electrode was introduced as a working electrode while Pt wire and Ag/AgCl served as counter and reference electrodes, respectively. The supporting electrolyte was 0.2 M $LiClO_4$ in aqueous solution of pH 1.8 $HClO_4$. Oxygen was removed from solution by purging with high purity nitrogen.

Photocurrent–photovoltage characteristics and photocurrent action spectra were measured in a sandwich-type cell; the sensitized electrode filled with electrolyte pressed against the Pt coated conducting glass electrode. The electrolyte solution consisted of 0.5 M LiI/0.05 M I_2 in 1:1 acetonitrile-NMO (3-methyl-2-oxazolidinone). Illumination of the cell was conducted from the nanoporous electrode side, using a 250 W xenon lamp, calibrated to one sun in the visible range. A 250 W xenon lamp coupled with a 4 nm bandwidth monochromator were used in the IPCE measurements.

For the dark current measurements, the conducting glass exposed area was blocked by insulating polymer, electrochemically polymerized prior to dye adsorption. The electropolymerization of the insulating polyphenoxide is described elsewhere [24].

An Eco Chemie Autolab 20 potentiostat was used for the electrochemical measurements.

3. Results and discussion

The results presented in this report summarize our understanding of the core–shell nanoporous electrode covering six systems. All six electrodes consist of a nanoporous TiO_2 matrix that is covered with a thin layer of a second wide band gap semiconductor. Two systems, the TiO_2–Nb_2O_5 and the TiO_2–$SrTiO_3$, were reported previously, showing different effects of the coating on the electrode properties. Here, we extend this study to a wider range of shell materials aimed at two goals: to gain better understanding of the core–shell system and to improve the conversion efficiency of DSSCs.

The coating effect in each core–shell system is based on a comparison between a set of bare TiO_2 electrodes and a set of core–shell ones. All the electrodes of such a comparison were made at the same time and experienced similar treatment including the second sintering cycle that followed the coating. Furthermore, only electrodes that exhibited similar absorption spectrum after the dye adsorption were included in these sets. Since a similar approach is not possible for the comparison between the different core–shell systems, we present the results in terms of percentage of change. That is, the change in cell performance due to the replacement of the standard bare electrode with the relevant core–shell one. We note, however, that all the reference cells, i.e. those containing the bare TiO_2 electrodes, were of the same quality yielding more than 3.5% efficiency.

Optimization of the core–shell electrodes was carried out using different coating conditions. The main parameters that were varied were the type of shell material precursor, its concentration, the hosting solvent, dipping duration and finally, the sintering temperature and duration. The results represent the core–shell electrodes that exhibited the largest effect on the DSSCs performance. The exact procedures are provided in the Section 2.

Table 1 shows the percentage of variation of the solar cell parameters resulting from the replacement of the bare TiO_2 electrode by the different core–shell electrodes. Four core–shell systems increase the overall conversion efficiency of the cell while the other two decrease the efficiency. One exception is the TiO_2–Nb_2O_5 system in which all cell parameters are improved by the coating resulting in the largest increment of the cell efficiency. In all other cases, the coatings involve different trends regarding the various cell parameters, which result in either an increase or a decrease of the conversion efficiency.

The case of the TiO_2–Nb_2O_5 system is discussed extensively elsewhere [20]. It was shown that the Nb_2O_5 shell forms an energy barrier at the TiO_2 electrolyte interface which reduces the rate of recombination between the photo-separated charges, i.e. the electron in the TiO_2 and the oxidized ions or dye. Consequently, both the electron accumulation and the electron collection efficiency are improved. The results presented in Table 1 seem to indicate that apart from the TiO_2–Nb_2O_5 case, coating does not create such an energy barrier at the electrode surface. Although, the open circuit photovoltage (V_{oc}) increases in most of the systems (as in the case of the barrier formation), at the same time (unlike the barrier case) the short circuit photocurrent (J_{sc}) decreases. Moreover, the largest V_{oc} increase induced by the coating is obtained for the TiO_2–ZnO system, although energy barrier fabrication in this system is not expected since the conduction band potentials of the core (TiO_2) and the shell (ZnO) are similar [1]. Thus, for these systems we adopt the bands shift mechanism previously suggested for the TiO_2–$SrTiO_3$ system [22]. According to this approach, the coating forms a dipole layer at the electrode/electrolyte interface which shifts the electrode bands potentials depending on the dipole intensity and direction. The dipole layer is attributed to either the different electron affinity or different acidity of the two semiconductors.

Table 1
The percentage of variation of the solar cell parameters resulting from the replacement of the bare TiO_2 electrode by the various core–shell electrodes

Shell material	Efficiency change (%)	V_{oc} change (%)	J_{sc} change (%)	FF change (%)
Nb_2O_5	37.3	10.4	11.8	10.8
ZnO	15.4	15.3	−3.1	3.2
$SrTiO_3$	15.2	8.9	−2.9	9.0
Al_2O_3	15.5	5.4	−3.2	13.2
ZrO_2	−10.6	4.5	−21.2	8.5
SnO_2	−45.3	−12.9	−35.3	−2.9

In the following sections, we support the band shift description by various measurements. In order to identify the controlling parameter we analyze the dependence of the solar cell parameters on two different properties of the core–shell materials; electron affinity and acidity. The dispassion is based on a representative system, the TiO_2–ZnO electrode, emphasizing that similar results were observed for all the systems presented in Table 1 except the TiO_2–Nb_2O_5 case.

3.1. Spectro-electrochemistry

The spectroelectrochemical measurements utilize undyed electrodes in aqueous supporting electrolyte. Upon application of negative potential, the electrons accumulated in the nanoporous electrode affect the absorption spectrum of the electrode [25,26]. The spectral changes are characterized by absorption bleach below 400 nm and a buildup of a wide absorption peak centered around 700 nm. The increase at longer wavelength is due to the absorption of the free electrons in the semiconductor while the bleach reflects electron accumulation in the conduction band. Fig. 1 shows the bleach region measured for bare TiO_2 and TiO_2–ZnO electrodes. The spectra represent the absorption change due to application of −0.9 V versus Ag/AgCl compared with open circuit conditions. Different electron accumulation in similar electrodes should be reflected in the width and intensity of the bleach [20]. Thus, the similarity of the two spectra presented in Fig. 1 indicates that both the bare TiO_2 and the TiO_2–ZnO electrode are capable of similar accumulation per a given potential. In other words, no barrier for electron leakage to solution is formed in this case.

3.2. Dark current

Dark current in DSSCs cannot be related directly to the recombination current since the electrolyte concentration in the porous film and the potential distribution across the nanoporous electrode in dark are different than those under illumination [6]. However a comparison between two similar cells can provide information regarding the relative recombination rates.

An insulating polymer was electrochemically deposited on the exposed area of the conducting substrate in order to eliminate the possibility that the measured current will be affected by different degree of coverage of the conducting substrate [24]. Fig. 2 presents the dark currents of the bare TiO_2 and the TiO_2–ZnO electrodes introduced to the DSSC. The ZnO shell shifts the onset potential to negative values while maintaining the curve shape. This behavior indicates that the ZnO does not generate a barrier which limits the electrons to the TiO_2 region but rather it shifts the conduction band potential negatively, determining lower electron density in the TiO_2 for any given applied potential. Consequently, the electron reaction with the ions in the electrolyte solution as a function of the electron density in the TiO_2 (rather than potential applied to the TiO_2) does not change upon coating.

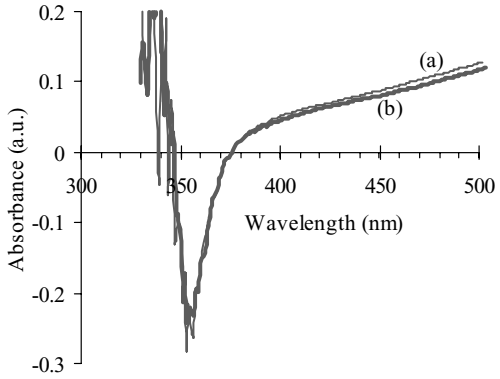

Fig. 1. The absorbance spectra at the bleach region of the (a) bare TiO_2 and (b) ZnO coated TiO_2 electrodes under applied potential of −0.9 V vs. SCE. The similarity of the two spectra indicates that both electrodes are capable of similar electron accumulation.

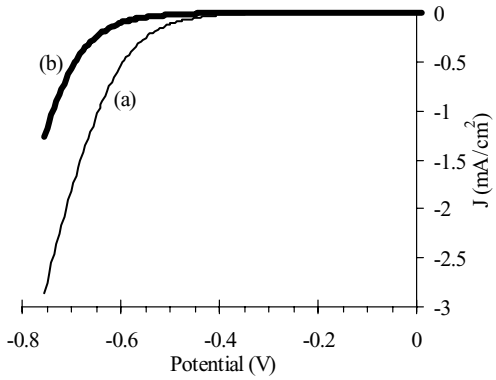

Fig. 2. Dark current of the (a) bare TiO_2 and (b) ZnO coated TiO_2 electrodes introduced to DSSCs. The ZnO shell shifts the onset potential to negative values while maintaining the curve shape.

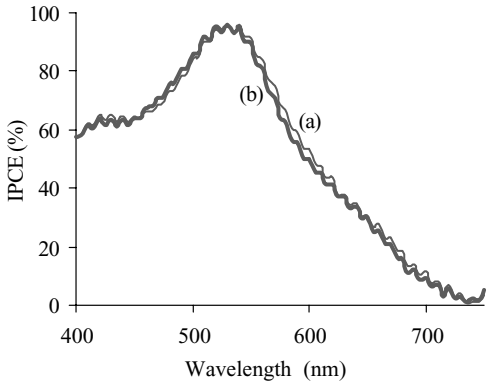

Fig. 3. The IPCE of two DSSCs consisting of the (a) bare TiO_2 and (b) ZnO coated TiO_2 electrodes. The similarity of the curves indicates that the recombination rate is not affected by the shell formation.

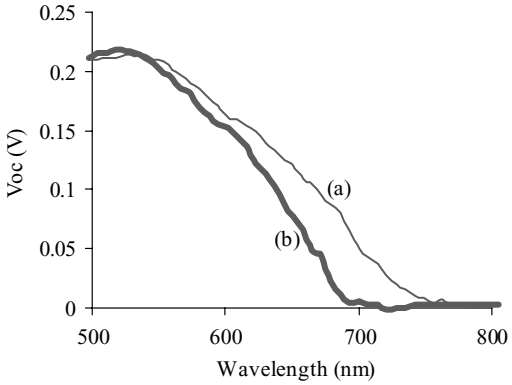

Fig. 4. V_{oc} as a function of the illumination wavelength for DSSCs containg (a) bare TiO_2 and (b) ZnO coated TiO_2 electrodes. Coating the TiO_2 electrode with ZnO shell shifts the onset of injection to shorter wavelength, indicating a shift of the TiO_2 conduction band in the negative direction.

3.3. Collection efficiency

Changes in the electron collection efficiency affect the shape of the incident photon to current efficiency spectrum. The effect is more pronounced at wavelengths of lower dye absorption since the electrons photo-injected at these wavelengths are generated at relatively large distances from the current collector, thus being highly sensitive to recombination processes. In practice, the improvement in the collection efficiency changes the IPCE values throughout the spectrum but the pronounced effect relates to the shape of the IPCE curve. Fig. 3 shows the IPCE curves of the bare TiO_2 and the TiO_2–ZnO systems normalized to 100% peak value. The curves are similar, indicating that the electron lifetime in the nanoporous electrode is not affected by the shell formation, as would be the case for surface energy barrier formation.

3.4. On-set of injection

The injection of electrons takes place only from dye excited states that are located above the conduction band edge. Therefore, at long wavelengths in which the dye is excited to states that are energetically positive of the conduction band edge, the generation of photovoltage and photocurrent will not occur. Since light harvesting by the dye at this wavelength region is not efficient, we utilized photovoltage spectroscopy rather than photocurrent spectroscopy to measure the onset of injection (the IPCE measurement is not sensitive in the long wavelength region due to the very low electron collection efficiency resulting from the light absorption profile and the low conductivity of the nanoporous network). In practice, a measurement of the open circuit photovoltage as a function of the illuminating wavelengths (scanning from the long wavelengths to the short ones to avoid charging effects) reveals the lowest dye excited state that injects into the semiconductor electrode. Fig. 4 presents the open circuit photovoltage spectra of the bare TiO_2 and the TiO_2–ZnO systems. The absorption spectra of the dye on both the bare and coated electrodes were similar. Fig. 4 shows that coating the TiO_2 electrode with ZnO shell shifts the onset of injection to a shorter wavelength. That is, the movement of the TiO_2 conduction band in the negative direction requires higher excitation energy to permit injection. Furthermore, the onset shift from 721 to 679 nm at photovoltage of 30 mV corresponds to a conduction band shift of 106 mV. This shift value correlates well with photovoltage measurements under white light illumination in which the photovoltage increased from 667 mV at the bare TiO_2 electrode to 769 mV for the ZnO coated TiO_2 electrode.

As mentioned above, the core–shell electrodes with the other materials, ZrO_2, Al_2O_3 and $SrTiO_3$ show similar behavior like the ZnO coated TiO_2 electrode. The presented results indicate that the main effect of the electrode coating is the movement of the TiO_2 conduction band. The formation of an energy barrier at the electrode/electrolyte interface was achieved only in the exceptional case of Nb_2O_5 shell. We relate the conduction band shift to the formation of surface dipole layer at the core–shell interface resulting from differences between the core and shell materials with respect to their acidity or electron affinity. Figs. 5 and 6 present the

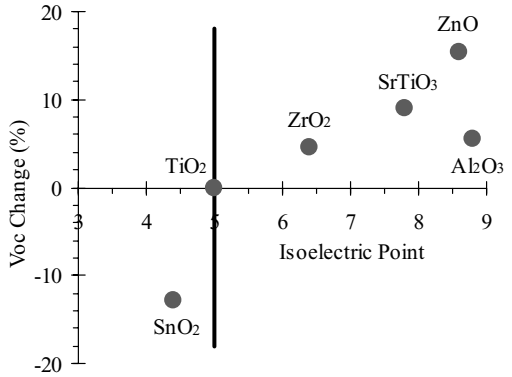

Fig. 5. The percentage of V_{oc} change upon coating as a function of the isoelectric point of the shell material. Shell with higher isoelectric point than TiO_2 generates a surface dipole directed toward the TiO_2, thus shifting the TiO_2 conduction band negatively.

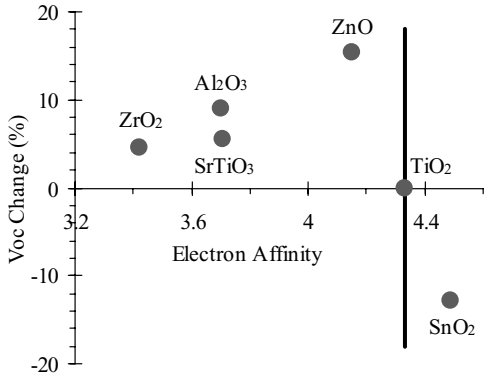

Fig. 6. The percentage of V_{oc} change upon coating as a function of the electron affinity of the shell. Shell with lower electron affinity than TiO_2 generates a surface dipole directed toward the TiO_2, thus shifting the TiO_2 conduction band negatively.

percentage of V_{oc} change upon coating as a function of the isoelectric point and the electron affinity of the shell [27–29]. When the isoelectric point of the shell is higher than that of the TiO_2, the shell material maintains a more positive surface with respect to the core TiO_2. Thus, a surface dipole directed towards the TiO_2 is generated. As shown in Fig. 5, a good correlation between the V_{oc} changes and the isoelectric point is observed. In the same manner, lower electron affinity of shell with respect to that of the core TiO_2 leads to a positive charging of the shell relative to the TiO_2 core. As a consequence, the TiO_2 conduction band shifts in the negative direction resulting in higher V_{oc} of the DSSC. In this case, the correlation between the V_{oc} changes and the electron affinity (Fig. 6) is poor. Therefore, it seems that the acidity of the material is the important factor regarding these specific core–shell systems. We note, however, that the results cannot exclude the electron affinity argument.

3.5. Applications for DSSCs

The small number of suitable semiconductors for DSSCs limits the possibilities to optimize the nanoporous electrode by replacing the sensitized material. Therefore, the above results provide a way to tune the properties of the suitable semiconductors in order to achieved higher DSSCs performance. For example, the negative movement of the TiO_2 conduction band, described above, increased the overall conversion efficiency of some of the DSSCs tested in this study via a large increase in the open circuit voltage. On the other hand, it is often required to shift the conduction band positively in order to enable the use of dyes having excited state potential that is too low for coupling with bare TiO_2. In such cases the inorganic coating can also be used to tune the bands to the optimal potential of each dye.

Another advantage of this configuration relates to the electrode structure and stability. Unlike organic dipoles that can also be adsorbed to the surface for similar effect the inorganic coat does not reduce the available dye binding site and is highly stable under operation conditions.

Acknowledgements

This research was funded by the Israel Science Foundation founded by The Israel Academy of Science and Humanities.

References

[1] A. Hagfeldt, M. Gratzel, Chem. Rev. 95 (1995) 49.
[2] B.A. Parkinson, M.T. Spitler, Electrochim. Acta 37 (1992) 943.
[3] R. Argazzi, C.A. Bignozzi, T.A. Heimer, G.J. Meyer, Inorg. Chem. 36 (1997) 2.
[4] P. Bonhote, J.E. Moser, N. Vlachopoulos, L. Walder, S.M. Zakiruddin, R. Humphry-Baker, P. Pechy, M. Gratzel, Chem. Commun. (1996) 10.
[5] A. Hagfeldt, S.E. Lindquist, M. Gratzel, Sol. Energy Mater. Sol. Cells 32 (1994) 245.
[6] A. Zaban, A. Meier, B.A. Gregg, J. Phys. Chem. B 101 (1997) 7985.
[7] J. Bisquert, G. Garcia-Belmonte, F. Fabregat-Santiago, J. Solid State Electrochem. 3 (1999) 337.
[8] Y. Tachibana, J.E. Moser, M. Gratzel, D. Klug, J.R. Durrant, J. Phys. Chem. 100 (1996) 20056.
[9] L. Kavan, M. Gratzel, S.E. Gilbert, C. Klemenz, H.J. Scheel, J. Am. Chem. Soc. 118 (1996) 6716.
[10] D. Cahen, G. Hodes, M. Gratzel, J.F. Guillemoles, I. Riess, J. Phys. Chem. B 104 (2000) 2053.
[11] A. Kay, M. Gratzel, Chem. Mater. 14 (2002) 2930.
[12] K. Tennakone, G. Kumara, I.R.M. Kottegoda, V.P.S. Perera, Chem. Commun. (1999) 15.
[13] K. Tennakone, J. Bandara, P.K.M. Bandaranayake, G.R.A. Kumara, A. Konno, Jpn. J. Appl. Phys. 40 (2001) L732.
[14] K. Tennakone, P.K.M. Bandaranayake, P.V.V. Jayaweera, A. Konno, G. Kumara, Physica E 14 (2002) 190.
[15] P.A. Sant, P.V. Kamat, Phys. Chem. Chem. Phys. 4 (2002) 198.
[16] I. Bedja, P.V. Kamat, J. Phys. Chem. 99 (1995) 9182.
[17] E. Palomares, J.N. Clifford, S.A. Haque, T. Lutz, J.R. Durrant, J. Am. Chem. Soc. 125 (2003) 475.
[18] C. Nasr, P.V. Kamat, S. Hotchandani, J. Phys. Chem. B 102 (1998) 10047.
[19] A. Zaban, S.G. Chen, S. Chappel, B.A. Gregg, Chem. Commun. (2000) 2231.
[20] S.G. Chen, S. Chappel, Y. Diamant, A. Zaban, Chem. Mater. 13 (2001) 4629.
[21] S. Chappel, S.G. Chen, A. Zaban, Langmuir 18 (2002) 3336.
[22] Y. Diamant, S.G. Chen, O. Melamed, A. Zaban, J. Phys. Chem. B 107 (2003) 1977.
[23] B. O'Regan, D.T. Schwartz, S.M. Zakeeruddin, M. Gratzel, Adv. Mater. 12 (2000) 1263.
[24] B.A. Gregg, F. Pichot, S. Ferrere, C.L. Fields, J. Phys. Chem. B 105 (2001) 1422.
[25] C.Y. Liu, A.J. Bard, J. Phys. Chem. 93 (1989) 3232.
[26] D. Fitzmaurice, Solar Energy Mater. Solar Cells 32 (1994) 289.
[27] S.R. Desai, W. Hongbin, C.M. Rohlfing, L.-S. Wang, J. Chem. Phys. 106 (1997) 1309.
[28] H.P. Maruska, A.K. Ghosh, Sol. Energy Mater. 1 (1979) 411.
[29] M.A. Butler, D.S. Ginley, J. Electrochem. Soc. 125 (1978) 228.